Electronic Supporting Information

Zwitterionic Iodonium Species Afford Halogen Bond-Based Porous Organic Frameworks

Natalia S. Soldatova,[a] Pavel S. Postnikov,*[a,b] Daniil M. Ivanov,[a,c] Oleg V. Semyonov,[a] Olga S. Kukurina,[a] Olga Guselnikova,[a,d] Yusuke Yamauchi[d,e], Thomas Wirth,[d] Viktor V. Zhdankin,[e] Mekhman S. Yusubov,[a] Rosa M. Gomila,[f] Antonio Frontera,[g] Giuseppe Resnati*[a,h] and Vadim Yu. Kukushkin*[c]

[a] *Research School of Chemistry and Applied Biomedical Sciences,Tomsk Polytechnic University, Tomsk 634034, Russian Federation, E-mail: postnikov@tpu.ru*

[b] *Department of Solid State Engineering, Institute of Chemical Technology, Prague 16628, Czech Republic*

[c] *Institute of Chemistry, Saint Petersburg State University, Saint Petersburg 199034, Russian Federation, E-mail: v.kukushkin@spbu.ru*

[d] *National Institute for Materials Science (NIMS), 1-1 Namiki, Tsukuba, Ibaraki 305-0044, Japan*

[e] *Australian Institute for Bioengineering and Nanotechnology (AIBN), The University of Queensland, Brisbane, QLD 4072, Australia*

[f] *School of Chemistry; Cardiff University, Park Place, Cardiff, UK*

[g] *Department of Chemistry and Biochemistry, University of Minnesota, Duluth, MN 55812, USA*

[h] *Serveis Científico-Tècnics; Universitat de les Illes Balears, Crta. de Valldemossa Km 7.5, 07122 Palma de Mallorca, Spain*

[i] *Departament de Química, Universitat de les Illes Balears, Crta. de Valldemossa Km 7.5, 07122 Palma de Mallorca, Spain*

[j] *NFMLab, Department of Chemistry, Materials and Chemical Engineering "Giulio Natta"; Politecnico di Milano, via Mancinelli 7, I-20131 Milano, Italy, E-mail: giuseppe.resnati@polimi.it*

Table of Contents

Section S1. Materials and instrumentation.

All reagents and solvents were obtained from commercial sources and used without further purification from freshly opened containers. *Melting points* were measured on a Stuart SMP30 apparatus in capillaries and are not corrected. *High resolution electrospray ionization (ESI) mass-spectra* were obtained on a Bruker maXis spectrometer equipped with an ESI source. The instrument was operated in positive ion mode using an *m/z* range 50–1200. The nebulizer gas flow was 1.0 bar and the drying gas flow was 4.0 L/min. *The NMR spectra* were recorded on a Bruker Avance 400 or Bruker Fourier 300 at ambient temperature; the residual solvent signal was used as the internal standard. *The DSC-TG experiments* were carried out on a SDTQ 600 instrument (TA Instruments) in the temperature range from 30 to 500 °C under argon atmosphere (100 mL min^{-1}) with a heating rate of 10 °C/min. *Scanning Electron Microscopy (SEM)* images were taken using FEI Quanta 200 3D scanning electron microscope. The scan of SEM was performed at an accelerating voltage (HV) of 20 kV. Samples were sputter-coated with gold before analysis to minimize electron charging effects. *X-ray diffraction (PXRD)* data were measured at room temperature using a Bruker D2 Phaser Desktop X-ray diffractometer equipped with a CuKα source (the data were collected in the range of 2θ = 5–32° with a step size of 0.02°(2θ)) or XRD-7000S (Shimadzu, Japan) with CuKα tube (40 kV, 30 mA) at the scanning range of 3–32 ° with a step size of 0.0143° (2θ). *FTIR spectra* were recorded on the Agilent Cary 630 spectrometer equipped by ATR accessory with 100 scans and 2 cm^{-1} resolution. The spectra were corrected using a straight baseline in the (4000–650) cm^{-1} spectral region. *VT-Raman spectroscopic* measurements were performed on a confocal Raman microscopy (NTEGRA SPECTRA) with an integrated thermal-controlled heating plate and with 633 nm laser set 0.32 μW with 5 scans for every measurement with acquisition time equal 15 s per scan. The laser beam was focused on the isolated crystal through 20X objective. Microcrystalline powder of **1a** was placed on the heating plate and the measurements were conducted at 25, 50, 100, and 140 °C after the temperature equilibration for 5 min.

The surface area, pore size distribution curve, and pore volume were determined from the nitrogen adsorption–desorption isotherm (Quantachrome Autosorb-iQ2, Boynton Beach, FL, USA) using the Brunauer−Emmett−Teller (BET) and Non-Local Density Functional Theory (NLDFT) methods. Before the measurement, the sample (approx. 27 mg) was placed in a glass cell and degassed at 80 °C in vacuo ($7 \cdot 10^{-6}$ $Torr^{-1}$) for 24 h.

Section S2. Synthesis of 4-(aryliodonio)benzenesulfonates and characterization of the products.

Among iodonium salts, zwitterionic species are rare and poorly studied. The reported examples include 3- and 4-(aryliodonio)carboxylates,[1,2] 4-(aryliodonio)sulfamides,[3,4] and 2-(aryliodonio)sulfonates,[5] 2-(aryliodonio)trifluoroborates[6] and *closo*-borate derivatives.[7] These zwitterions were prepared using such strong oxidant as $K_2S_2O_8$ in H_2SO_4[1,3,4] or Selectfluor®.[6] We developed an easy approach toward a series of novel zwitterionic 4-(aryliodonio)benzenesulfonates from the readily available 4-iodobenzenesulfonic acid.[8] Owing to the presence of the electron withdrawing (EWG) SO_3H-group, we employed Oxone® ($2KHSO_5 \cdot KHSO_4 \cdot K_2SO_4$) in the presence of sulfuric acid as an oxidant (for the relevant applications of Oxone® and $K_2S_2O_8$ see refs.[1,3,4,9–14]). According to the optimized procedure, the finely ground Oxone® was mixed with 4-iodobenzensulfonic acid in acetonitrile solution of conc. H_2SO_4 and the reaction was stirred for 12 h at RT (**Scheme 1**). The addition of water, once the reaction is complete, led to the isolation of **1** (74%) and **2** (60%). The reaction with electron poor chlorobenzene employing Oxone in conc. H_2SO_4[9,10] allows for the preparation of target compound **3** in almost quantitative yields.

Synthetic work

General procedure for the synthesis of 1–2. Sulfuric acid (240–500 μL) was added dropwise to a mixture of 4-iodobenzenesulfonic acid (1 mmol, 284 mg) and finely crushed Oxone (1 mmol, 615 mg) in MeCN (2 ml) at 0–5 °C. Then corresponding arene (1.1–1.5 mmol) was added, and the reaction mixture was stirred overnight at ambient temperature. MeCN was removed by rotary evaporation, then water (10 mL) and Et_2O (2 mL) was poured to the reaction mixture. The formed precipitate was filtered off and washed with water (3×5 mL), hexane (3×5 mL). The obtained crystalline product was dried in the air at ambient temperature.

4-(mesityliodonio)benzenesulfonate (**1**). The reaction of 4-iodobenzenesulfonic acid (1 mmol, 284 mg), mesitylene (1.1 mmol, 150 μL), Oxone (1 mmol, 615 mg) and sulfuric acid (240 μL) accordingly to the general procedure afforded 297 mg (74%) of **1** isolated as the colorless crystalline solid; mp 179–181 °C. ^{1}H NMR (400 MHz, DMSO-d_6) δ 7.94 (d, J = 8.4 Hz, 2H), 7.65 (d, J = 8.4 Hz, 2H), 7.21 (s, 2H), 2.60 (s, 6H), 2.29 (s, 3H). ^{13}C{^{1}H} NMR (100 MHz, DMSO-d_6) δ: 151.2, 143.1, 141.5, 134.3, 129.8, 128.7, 122.8, 114.3, 26.3, 20.5. HRESIMS$^+$: m/z calcd. for $[M+H]^+$ $C_{15}H_{16}IO_3S^+$: 402.9859, found 402.9833.

4-((2,5-dimethylphenyl)iodonio)benzenesulfonate (**2**). The reaction of 4-iodobenzenesulfonic acid (1 mmol, 284 mg), *p*-xylene (1.5 mmol, 184 μL), Oxone (1 mmol, 615 mg) and sulfuric acid (500 μL) accordingly to the general procedure afforded 236 mg (61%) of **2** isolated as the colorless crystalline solid; mp 217–219 °C (decomp.). ^{1}H NMR (300 MHz, DMSO-d_6) δ 8.22 (s, 1H), 8.14 (d, J = 8.4 Hz, 2H), 7.65 (d, J = 8.1 Hz, 2H), 7.43 (d, J = 7.8 Hz, 2H), 7.38 (d, J = 7.8 Hz, 2H), 2.55 (s, 3H), 2.30 (s, 3H). ^{13}C{^{1}H} NMR (75 MHz, DMSO-d_6) δ: 151.3, 139.3, 137.4, 137.1, 134.9, 133.6, 131.2, 128.8, 121.3, 115.6, 24.6, 20.2. HRESIMS$^+$: m/z calcd. for $[M+H]^+$ $C_{14}H_{14}IO_3S^+$: 388.9708, found 388.9702.

General procedure for the synthesis of 3. Sulfuric acid (800 μL) was added dropwise to a mixture of 4-iodobenzenesulfonic acid (1 mmol, 284 mg) and finely crushed Oxone (1 mmol, 615 mg) at 0–5 °C. Then corresponding arene (3 mmol, 304 μL) was added, and the reaction mixture was stirred overnight at ambient temperature. Water (10 mL) was poured to the reaction mixture and the formed precipitate was filtered off and washed with water (3×5 mL), hexane (3×5 mL) acetone (5 mL). The obtained crystalline product was dried in the air at ambient temperature. The product **3** was isolated as the colorless crystalline solid 386 mg (98%); mp 279–281 °C (decomp.). ^{1}H NMR (300 MHz, DMSO-d_6) δ: 8.24 (d, J = 8.4 Hz, 2H), 8.20 (d, J = 8.4 Hz, 2H), 7.67 (d, J = 8.4 Hz, 2H), 7.61 (d, J = 8.7 Hz, 2H). ^{13}C{^{1}H} NMR (75 MHz, DMSO-d_6) δ: 151.6, 137.4, 137.0, 135.0, 131.8, 128.7, 116.5, 114.6. HRESIMS$^+$: m/z calcd. for $[M+H]^+$ $C_{12}H_9ClIO_3S^+$: 394.9006, found 394.9004.

Section S3. Crystal growth and X-ray structure determinations

Crystals of **1a**–**b** and **2** suitable for XRD (**Schemes 1**) were grown by dissolution of the samples in hot aqueous MeOH followed by crystallization upon slow evaporation at 20–25 °C. Crystals of **3** were prepared by slow vapor diffusion of MeOH into a DMSO solution of the compound at ambient conditions.

X-ray diffraction data were collected at 100 K on a SuperNova, Dual, Cu at zero, Atlas diffractometer using Cu Kα (λ = 1.54184 Å; **1a**) or Mo Kα (λ = 0.71073 Å; **1b**) radiation or on a SuperNova, Single source at offset/far, HyPix3000 diffractometer using Cu Kα (λ = 1.54184 Å; **2, 3**). The structures were solved with the ShelXT[15] structure solution program using Intrinsic Phasing and refined with the ShelXL[16] refinement package incorporated in the OLEX2 program package[17] using Least Squares minimization. The carbon-bound H atoms were placed in calculated positions. Empirical absorption correction was applied in CrysAlisPro[18] program complex using spherical harmonics, implemented in SCALE3 ABSPACK scaling algorithm. The unit cells of **1a** and **1b** also contains disordered molecules of H_2O (total potential solvent accessible void volume per cell is 2012 and 760 $Å^3$, respectively; electron count per cell is 485 and 219 electrons, correspondingly) that have been treated as a diffuse contribution to the overall scattering without specific atom positions using SQUEEZE/PLATON.[19] XRD data and structural refinement parameters for **1a**, **1b**, **2**, and **3** are summarized in **Table S1**. Supplementary crystallographic data have been deposited at Cambridge Crystallographic Data Centre (CCDC 2096180, 2096183, 2096184, 2096193) and can be obtained free of charge via www.ccdc.cam.ac.uk/data request/cif.

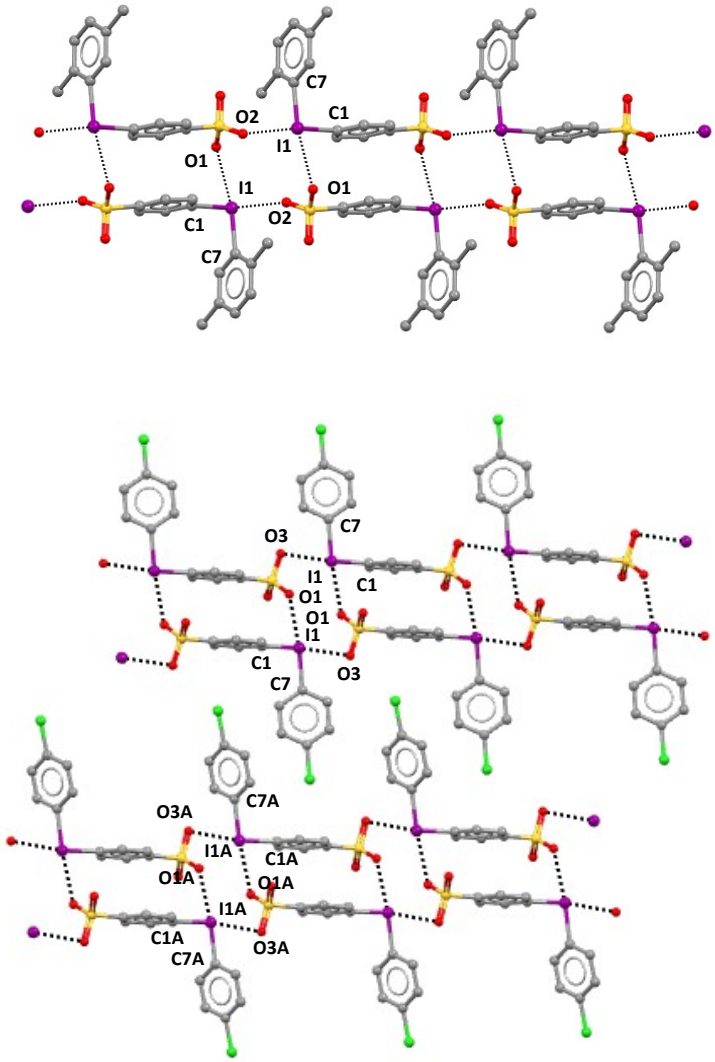

Figure S1. Partial representation (Mercury 4.3.1, ball and stick) of the crystal packing of **2** (top panel) and **3** (bottom panel) evidencing the ribbons present in the respective lattices. Hydrogen atoms are omitted; XB are dashed black lines. Color coding: grey, carbon; red, oxygen; ocher, sulfur; violet, iodine.

Table S1. Crystal data and structure refinement for **1a**, **1b**, **2**, and **3**.

Identification code	**1a**	**1b**	**2**	**3**
CCDC number	2096180	2096183	2096184	2096193
Empirical formula	$C_{15}H_{15}IO_3S$	$C_{15}H_{15}IO_3S$	$C_{14}H_{13}O_3SI$	$C_{12}H_8ClIO_3S$
Formula weight	402.23	402.23	388.20	394.59
Temperature, K	100(2)	100(2)	100(2)	100(2)
Crystal system	trigonal	triclinic	monoclinic	triclinic
Space group	R-3	P-1	$P2_1/c$	P-1
a, Å	20.7704(4)	10.1666(2)	7.09640(10)	6.09810(10)
b, Å	20.7704(4)	14.3384(3)	23.1449(4)	8.11370(10)
c, Å	21.5736(4)	20.5652(3)	8.14500(10)	25.8853(3)
α, °	90	84.4790(10)	90	94.9610(10)
β, °	90	82.633(2)	97.033(2)	93.9970(10)
γ, °	120	74.902(2)	90	91.8580(10)
Volume, $Å^3$	8060.1(3)	2864.29(10)	1327.71(3)	1271.90(3)
Z	18	6	4	4
ρ_{calc}, g/cm^3	1.492	1.399	1.942	2.061
μ, mm^{-1}	15.173	1.789	20.441	23.243
F(000)	3564.0	1188.0	760.0	760.0
Crystal size, mm^3	0.2 × 0.11 × 0.10	0.36 × 0.13 × 0.11	0.406 × 0.229 × 0.079	0.185 × 0.109 × 0.048
Radiation	CuKα (λ = 1.54184)	MoKα (λ = 0.71073)	Cu Kα (λ = 1.54184)	Cu Kα (λ = 1.54184)
2Θ range for data collection, °	9.56 to 129.984	6.006 to 63.82	7.64 to 140.864	3.436 to 140.844
Index ranges	$-24 \le h \le 24$, $-24 \le k \le 13$, $-25 \le l \le 25$	$-13 \le h \le 15$, $-20 \le k \le 21$, $-29 \le l \le 29$	$-8 \le h \le 8$, $-28 \le k \le 28$, $-9 \le l \le 7$	$-7 \le h \le 7$, $-9 \le k \le 9$, $-31 \le l \le 31$
Reflections collected	12896	61898	7808	24149
Independent reflections	3034 [R_{int} = 0.0399, R_{sigma} = 0.0261]	17510 [R_{int} = 0.0263, R_{sigma} = 0.0239]	2531 [R_{int} = 0.0702, R_{sigma} = 0.0476]	4848 [R_{int} = 0.0522, R_{sigma} = 0.0317]
Data/restraints/parameters	3034/0/184	17510/18/547	2531/0/174	4848/0/325
Goodness-of-fit on F^2	1.058	1.017	1.033	1.083
Final R indexes [I≥2σ (I)]	R_1 = 0.0273, wR_2 = 0.0710	R_1 = 0.0308, wR_2 = 0.0706	R_1 = 0.0498, wR_2 = 0.1343	R_1 = 0.0442, wR_2 = 0.1211
Final R indexes [all data]	R_1 = 0.0283, wR_2 = 0.0718	R_1 = 0.0362, wR_2 = 0.0733	R_1 = 0.0511, wR_2 = 0.1364	R_1 = 0.0462, wR_2 = 0.1228
Largest diff. peak/hole, $e \cdot Å^{-3}$	1.53/–0.67	1.65/–2.30	1.80/–2.20	1.94/–1.42

Section S4. XRD patterns of 1b

Crystals of **1a** and **1b** exhibited different stabilities after their separation from the corresponding mother liquors. Crystalline powder of **1a** was isolated in a pure form and the corresponding XRD pattern (**Fig. S2**) is in a good agreement with the simulated pattern. By contrast, the XRD pattern **1b**, after its separation and drying, demonstrated the degradation of the pristine crystal structure.

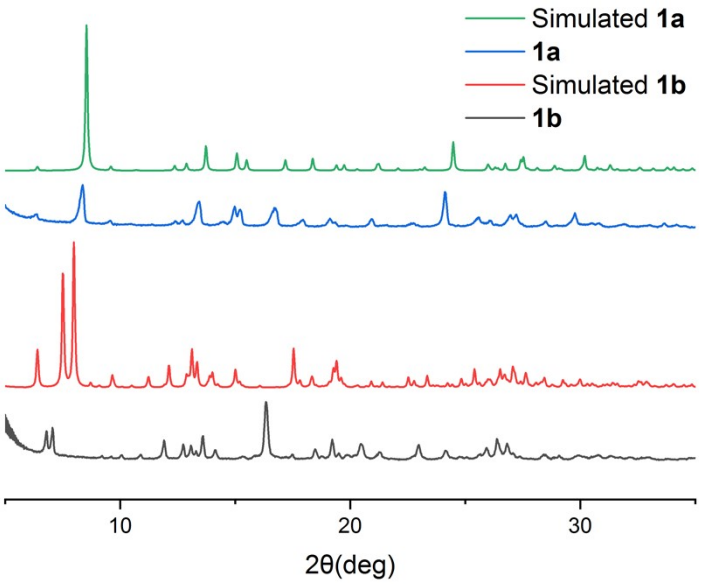

Figure S2. The comparison between the simulated XRD patterns of **1a** and **1b**. The experimental diffraction curves were recorded after the isolation and drying.

Section S5. Adsorption properties of 1a

Repeated adsorption–desorption of water

Screw-necked vial with 100 mg of preliminary dried XOF **1a** was put for 2 h in a desiccator with water placed on its bottom part, whereupon this sample was kept in air for 2 h until the constant weight. After a gravimetrical determination of adsorbed water, the sample was dried at 140 °C for 30 min followed its by cooling to RT in a sealed vial. Five cycles of adsorption–desorption were performed for 3 samples. The amount of adsorbed water was represented as an uptake in mg/g of the sample.

Adsorption of D_2O

Sample of **1a** was dried at 140 °C for 30 min, whereupon it was placed in desiccator with D_2O on its bottom part for 2 h and then the sample was kept in air for 2 h until constant weight. Samples of pristine and dried XOF were then studied by FTIR ATR spectroscopy.

Table S2. FTIR peak and their assignment

Peak positions, cm^{-1}	Assignment
3435	O–H inside pores
3100–3000	=C–H stretch in aromatic
2990–2820	CH_3 *antysym* and *sym* stretching in mesitylene
2530	D_2O stretch
1646	benzene ring stretch
1567	benzene ring stretch
1456	CH_3 *antisym* deformation
1382	CH_3 *sym* deformation
1303	v C–CH_3 of mesytelene
1278	vC–CH_3 of mesytelene
1181	S=O stretch in sulfonic acids
1108 and 1124	Aromatic C–H in plane bending vibration and C=S stretch in thiocarbonyl compounds
1027	SO_3 *sym* stretch in sulfonic acids
986	ring breathing mode of carbon ring
943	vC–CH_3 of mesytelene
853	C–H out of plane deformation 1,3,5-trisubstituted benzenes
820	C–H out of plane deformation 4-SO_3-substituted benzenes
732	C–H deformation

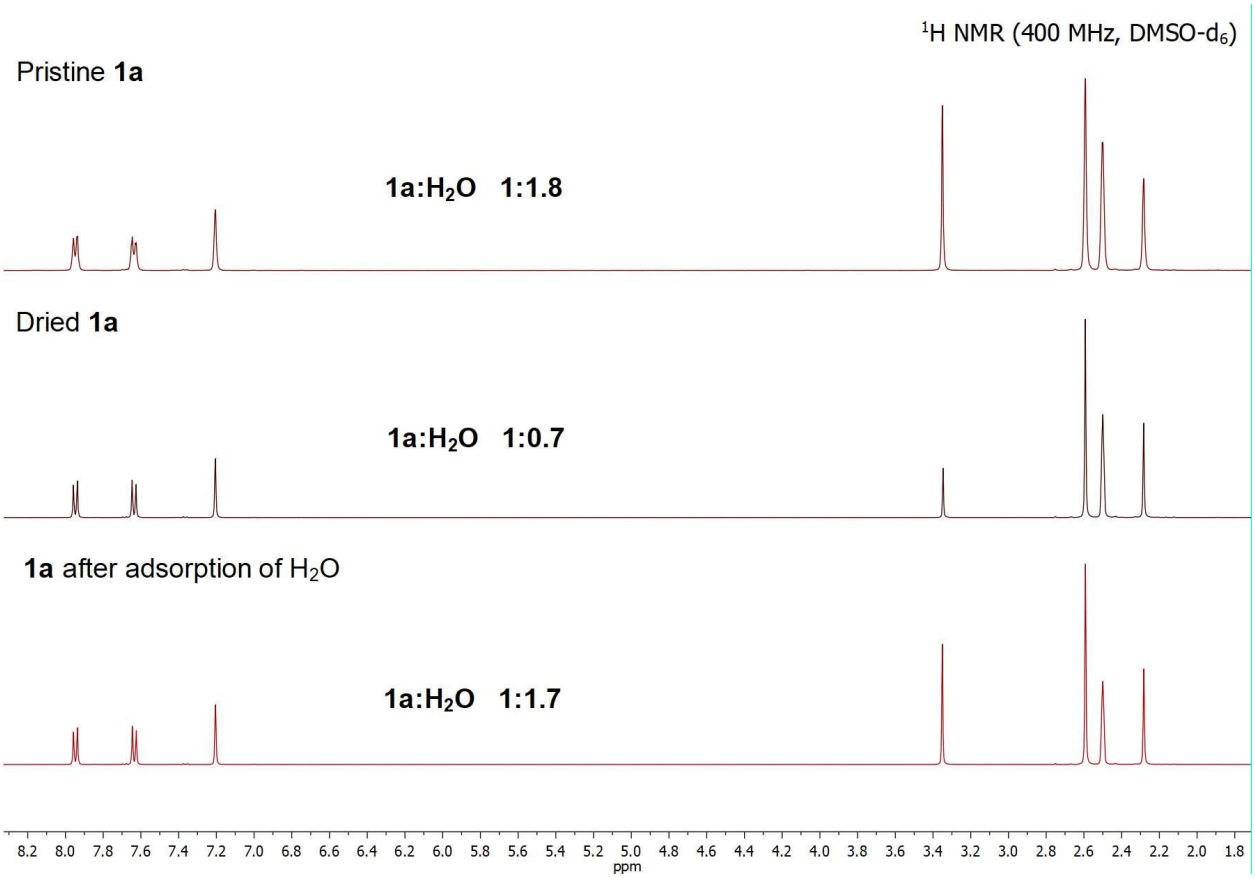

Figure S3. Determination of **1a**:H_2O ratio by NMR spectroscopy; the ratio is based on remaining water in DMSO-d_6. Residue peak of DMSO was used as an internal standard.

Section S6. Computational details

The calculations of the assemblies shown in **Figures 6–7, SA** and **SB** were performed at the DFT level of theory using PBE0 functional,[20] the def2-TZVP basis set[21] and the D3 dispersion correction[2255] with the help of the Gaussian-16 package.[23] The topological analysis of the electron density distribution has been analyzed with the help of the atoms in molecules (QTAIM) method developed by Bader[24] as well as noncovalent interaction plot (NCIPlot)[25,26] by using the AIMAll program.[27] The estimation of the individual XB energies was carried out using the QTAIM method and the V(r) predictor as recently proposed in the literature [$E = 0.778 \cdot V(r)$][28] for the PBE0 functional. The HB energies were estimated using the equation proposed by Espinosa *et al*. [$E = 0.5 \cdot V(r)$].[29] The MEP surfaces were computed at the PBE0-D3/def2-TZVP level of theory by means of the Gaussian-16 program.[56] The MEP plots of **Figure 5** were represented using the 0.001 au isosurface.

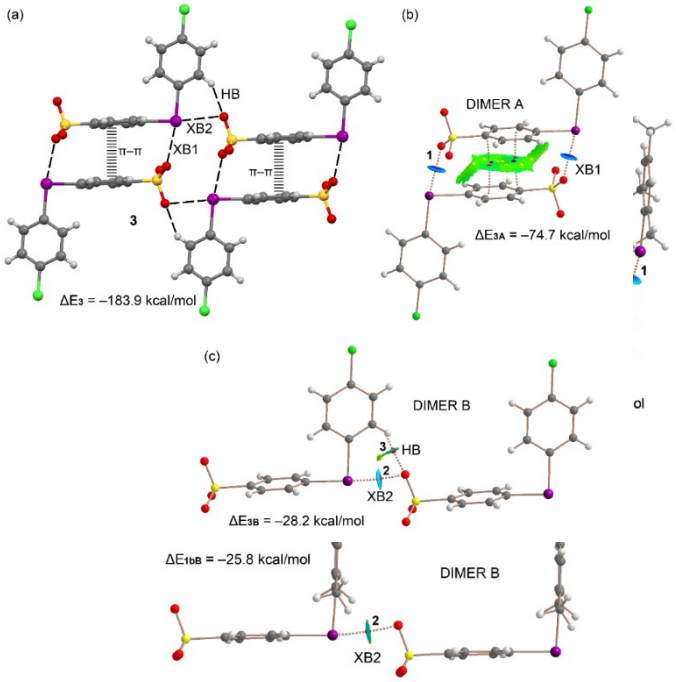

Figure S4. (a) Tetrameric assembly extracted from the X-ray structure of **1b**; (b,c) Combined QTAIM (bond CP in red, ring CP in yellow and cage CP in blue) and NCIplot (isosurface 0. 45 au, gradient cut-off 0.04 au, color range $-0.03 < \text{sign}(\lambda_2)\cdot\rho < 0.03$) of dimer **A** (b) and **B** (c). Only intermolecular interactions are shown.

Figure S5. (a) Tetrameric assembly extracted from the X-ray structure of **3**; (b,c) Combined QTAIM (bond CP in red, ring CP in yellow and cage CP in blue) and NCIplot (isosurface 0.45 au, gradient cut-off 0.04 au, color range $-0.03 < \text{sign}(\lambda_2)\cdot\rho < 0.03$) of dimer **A** (b) and **B** (c). Only intermolecular interactions are shown.

In general, the interaction energies of the assemblies analyzed for compounds **1**–**3** are very large because of the zwitterionic nature of these compounds. We also calculated the energies of the individual XBs and HBs in these assemblies by using the QTAIM parameters and the V_r energy predictor. This method is convenient to evaluate the energy associated to the interactions without the large contribution of purely electrostatic effects ($SO_3^{-}\cdots I^{+}$). The QTAIM parameters associated to the bond CPs numbered **1**–**3** in **Figures 6**–**7**, **S4** and **S5** are summarized in **Table S3**. For compound **1a**, both XBs are energetically similar (6.44 and 6.11 kcal/mol for XB1 and XB2, respectively) in agreement with the similar experimental distances (**Table 1**). The energy of the H-bond resulting in the bond CP#3 in dimer **B** is very small (0.66 kcal/mol), thus revealing that its contribution is negligible. For the rest of compounds, the XB1 is around 2 kcal/mol stronger than XB2, also in agreement with the experimental distances. The XB1 energy (labelled as bond CP#1) ranges from 6.5 kcal/mol in **1b** to 9.6 kcal/mol in **3**, and the XB2 energy (CP#2) ranges from 4.3 kcal/mol in **1b** to 6.3

kcal/mol in **3**, in line with the MEP values at both *σ*hs that increase on going from compound **1** to **3** (**Table 2**). Finally, in the case of dimer **B** of compound **3**, the HB is moderately strong (2.70 kcal/mol), thus also contributing to the stabilization of the dimer.

Table S3. QTAIM parameters (ρ, $\nabla^2\rho$, V_r, G_r in au) at the bond CPs labelled in **Figures 6**–**7**, **S4** and **S5**, and the dissociation energies (E_{dis}, kcal/mol) estimated using the potential energy density predictor for compounds **1**–**3**.

Compound	**ρ**	**$\nabla^2\rho$**	**V_r**	**G_r**	**E_{dis}**
1a					
CP #1 (Dimer A)	0.0229	0.0692	–0.0154	0.0164	7.5
CP #2 (Dimer B)	0.0217	0.0670	–0.0146	0.0157	7.1
CP #3 (Dimer B)	0.0044	0.0159	–0.0021	0.0030	0.7
1b					
CP #1 (DIMER A)	0.0204	0.0639	–0.0133	0.0146	6.5
CP #2 (DIMER B)	0.0148	0.0487	–0.0088	0.0105	4.3
2					
CP #1 (DIMER A)	0.0214	0.0644	–0.0138	0.0150	6.7
CP #2 (DIMER B)	0.0164	0.0547	–0.0102	0.0119	5.0
CP #3 (DIMER B)	0.0063	0.0182	–0.0023	0.0034	0.7
3					
CP #1 (DIMER A)	0.0278	0.0789	–0.0197	0.0197	9.6
CP #2 (DIMER B)	0.0205	0.0549	–0.0135	0.0148	6.6
CP #3 (DIMER B)	0.0125	0.0643	–0.0086	0.0112	2.7

References

1 S. V. Luis, F. Gaviña, P. Ferrer, V. S. Safont, M. C. Torres and M. I. Burguette, Non concerted pathways in the generation of dehydroarenes by thermal decomposition of diaryliodonium carboxylates., *Tetrahedron*, 1989, **45**, 6281–6296.

2 F. M. Beringer and I. Lillien, Diaryliodonium Salts. XIII. Salts in which the Cations Bear Carboxyl, Hydroxyl, Alkoxyl or Amino Groups 1,2, *Journal of the American Chemical Society*, 1960, **82**, 725–731.

3 D. D. DesMarteau, W. T. Pennington, V. Montanari and B. H. Thomas, Iodonium zwitterions, *Journal of Fluorine Chemistry*, 2003, **122**, 57–61.

4 H. Mei and D. D. DesMarteau, Bis(diaryliodonium) perfluorosulfonimide zwitterions as potential photo acid generators, *Journal of Fluorine Chemistry*, 2014, **160**, 12–15.

5 M. W. Justik, J. D. Protasiewicz and J. B. Updegraff, Preparation and X-ray structures of 2-[(aryl)iodonio]benzenesulfonates: novel diaryliodonium betaines, *Tetrahedron Letters*, 2009, **50**, 6072–6075.

6 R. Robidas, V. Guérin, L. Provençal, M. Echeverria and C. Y. Legault, Investigation of Iodonium Trifluoroborate Zwitterions as Bifunctional Arene Reagents, *Organic Letters*, 2017, **19**, 6420–6423.

7 P. Kaszyński and B. Ringstrand, Functionalization of closo -Borates via Iodonium Zwitterions, *Angewandte Chemie*, 2015, **127**, 6676–6681.

8 M. S. Yusubov, R. Y. Yusubova, V. N. Nemykin, A. V. Maskaev, M. R. Geraskina, A. Kirschning and V. V. Zhdankin, Potassium 4-Iodylbenzenesulfonate: Preparation, Structure, and Application as a Reagent for Oxidative Iodination of Arenes, *European Journal of Organic Chemistry*, 2012, **2012**, 5935–5942.

9 M. S. Yusubov, N. S. Soldatova, P. S. Postnikov, R. R. Valiev, D. Y. Svitich, R. Y. Yusubova, A. Yoshimura, T. Wirth and V. V. Zhdankin, Reactions of 1-Arylbenziodoxolones with Azide Anion: Experimental and Computational Study of Substituent Effects, *European Journal of Organic Chemistry*, 2018, **2018**, 640–647.

10 M. S. Yusubov, R. Y. Yusubova, V. N. Nemykin and V. V. Zhdankin, Preparation and X-ray Structural Study of 1-Arylbenziodoxolones, *The Journal of Organic Chemistry*, 2013, **78**, 3767–3773.

11 P. S. Postnikov, O. A. Guselnikova, M. S. Yusubov, A. Yoshimura, V. N. Nemykin and V. V. Zhdankin, Preparation and X-ray Structural Study of Dibenziodolium Derivatives, *The Journal of Organic Chemistry*, 2015, **80**, 5783–5788.

12 N. Soldatova, P. Postnikov, O. Kukurina, V. V Zhdankin, A. Yoshimura, T. Wirth and M. S. Yusubov, One-pot synthesis of diaryliodonium salts from arenes and aryl iodides with Oxone-sulfuric acid., *Beilstein journal of organic chemistry*, 2018, **14**, 849–855.

13 N. S. Soldatova, P. S. Postnikov, M. S. Yusubov and T. Wirth, Flow Synthesis of Iodonium Trifluoroacetates through Direct Oxidation of Iodoarenes by Oxone®, *European Journal of Organic Chemistry*, 2019, **2019**, 2081–2088.

14 N. Soldatova, P. Postnikov, O. Kukurina, V. V. Zhdankin, A. Yoshimura, T. Wirth and M. S. Yusubov, Facile One-Pot Synthesis of Diaryliodonium Salts from Arenes and Aryl Iodides with Oxone, *ChemistryOpen*, 2017, **6**, 18–20.

15 G. M. Sheldrick, SHELXT – Integrated space-group and crystal-structure determination, *Acta Crystallographica Section A Foundations and Advances*, 2015, **71**, 3–8.

16 G. M. Sheldrick, Crystal structure refinement with SHELXL, *Acta Crystallographica Section C Structural Chemistry*, 2015, **71**, 3–8.

17 O. V. Dolomanov, L. J. Bourhis, R. J. Gildea, J. A. K. Howard and H. Puschmann, OLEX2 : a complete structure solution, refinement and analysis program, *Journal of Applied Crystallography*, 2009, **42**, 339–341.

18 Agilent Technologies, *Technologies UK Ltd, Yarnton, Oxford, UK*, 2013.
19 A. L. Spek, PLATON, A Multipurpose Crystallographic Tool, Utrecht University, Utrecht, The Netherlands, 2005.
20 C. Adamo and V. Barone, Toward reliable density functional methods without adjustable parameters: The PBE0 model, *The Journal of Chemical Physics*, 1999, **110**, 6158–6170.
21 F. Weigend, Accurate Coulomb-fitting basis sets for H to Rn, *Physical Chemistry Chemical Physics*, 2006, **8**, 1057.
22 S. Grimme, J. Antony, S. Ehrlich and H. Krieg, A consistent and accurate ab initio parametrization of density functional dispersion correction (DFT-D) for the 94 elements H-Pu, *The Journal of Chemical Physics*, 2010, **132**, 154104.
23 M. J. Frisch, G. W. Trucks, H. B. Schlegel, G. E. Scuseria, M. A. Robb, J. R. Cheeseman, G. Scalmani, V. Barone, G. A. Petersson, H. Nakatsuji, X. Li, M. Caricato, A. V. Marenich, J. Bloino, B. G. Janesko, R. Gomperts, B. Mennucci, H. P. Hratchian, J. V. Ortiz, A. F. Izmaylov, J. L. Sonnenberg, D. Williams-Young, F. Ding, F. Lipparini, F. Egidi, J. Goings, B. Peng, A. Petrone, T. Henderson, D. Ranasinghe, V. G. Zakrzewski, J. Gao, N. Rega, G. Zheng, W. Liang, M. Hada, M. Ehara, K. Toyota, R. Fukuda, J. Hasegawa, M. Ishida, T. Nakajima, Y. Honda, O. Kitao, H. Nakai, T. Vreven, K. Throssell, J. A. Montgomery, J. E. Peralta, F. Ogliaro, M. J. Bearpark, J. J. Heyd, E. N. Brothers, K. N. Kudin, V. N. Staroverov, T. A. Keith, R. Kobayashi, J. Normand, K. Raghavachari, A. P. Rendell, J. C. Burant, S. S. Iyengar, J. Tomasi, M. Cossi, J. M. Millam, M. Klene, C. Adamo, R. Cammi, J. W. Ochterski, R. L. Martin, K. Morokuma, O. Farkas, J. B. Foresman and D. J. Fox, *Gaussian 16, Revision C.01, Gaussian, Inc., Wallingford, CT*, 2016.
24 R. F. W. Bader, A quantum theory of molecular structure and its applications, *Chemical Reviews*, 1991, **91**, 893–928.
25 E. R. Johnson, S. Keinan, P. Mori-Sánchez, J. Contreras-García, A. J. Cohen and W. Yang, Revealing Noncovalent Interactions, *Journal of the American Chemical Society*, 2010, **132**, 6498–6506.
26 J. Contreras-García, E. R. Johnson, S. Keinan, R. Chaudret, J.-P. Piquemal, D. N. Beratan and W. Yang, NCIPLOT: A Program for Plotting Noncovalent Interaction Regions, *Journal of Chemical Theory and Computation*, 2011, **7**, 625–632.
27 T. A. Keith, AIMALL (Version 19.02.13), *AIMALL (Version 19.02.13), TK Gristmill Software, Overland Park KS, USA,* 2019, (aim.tkgristmill.com).
28 L. E. Zelenkov, D. M. Ivanov, E. K. Sadykov, N. A. Bokach, B. Galmés, A. Frontera and V. Yu. Kukushkin, Semicoordination Bond Breaking and Halogen Bond Making Change the Supramolecular Architecture of Metal-Containing Aggregates, *Crystal Growth & Design*, 2020, **20**, 6956–6965.
29 E. Espinosa, E. Molins and C. Lecomte, Hydrogen bond strengths revealed by topological analyses of experimentally observed electron densities, *Chemical Physics Letters*, 1998, **285**, 170–173.

NMR spectra of 1–3

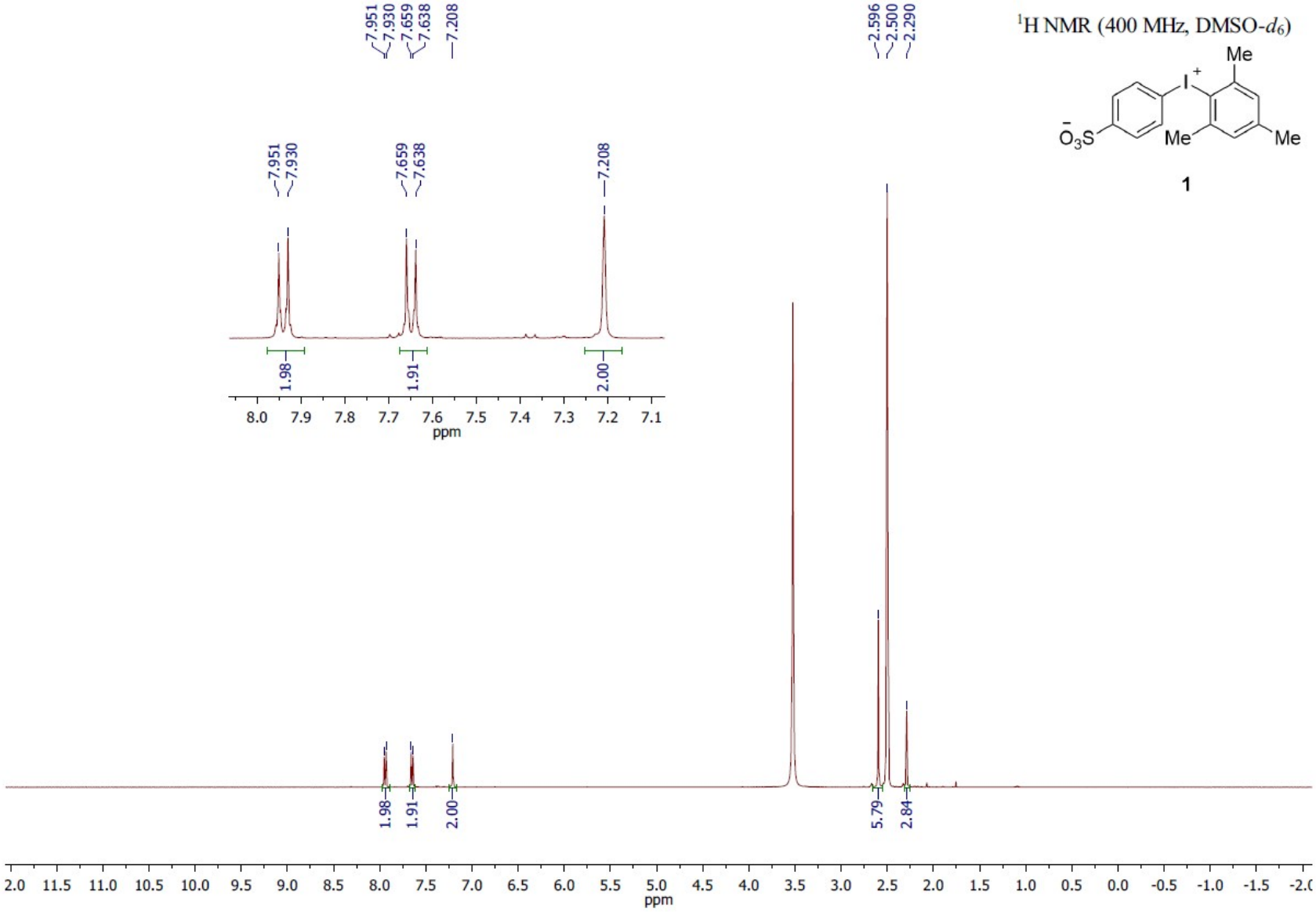

^{13}C NMR (100 MHz, DMSO-d_6)

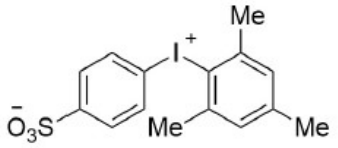

1

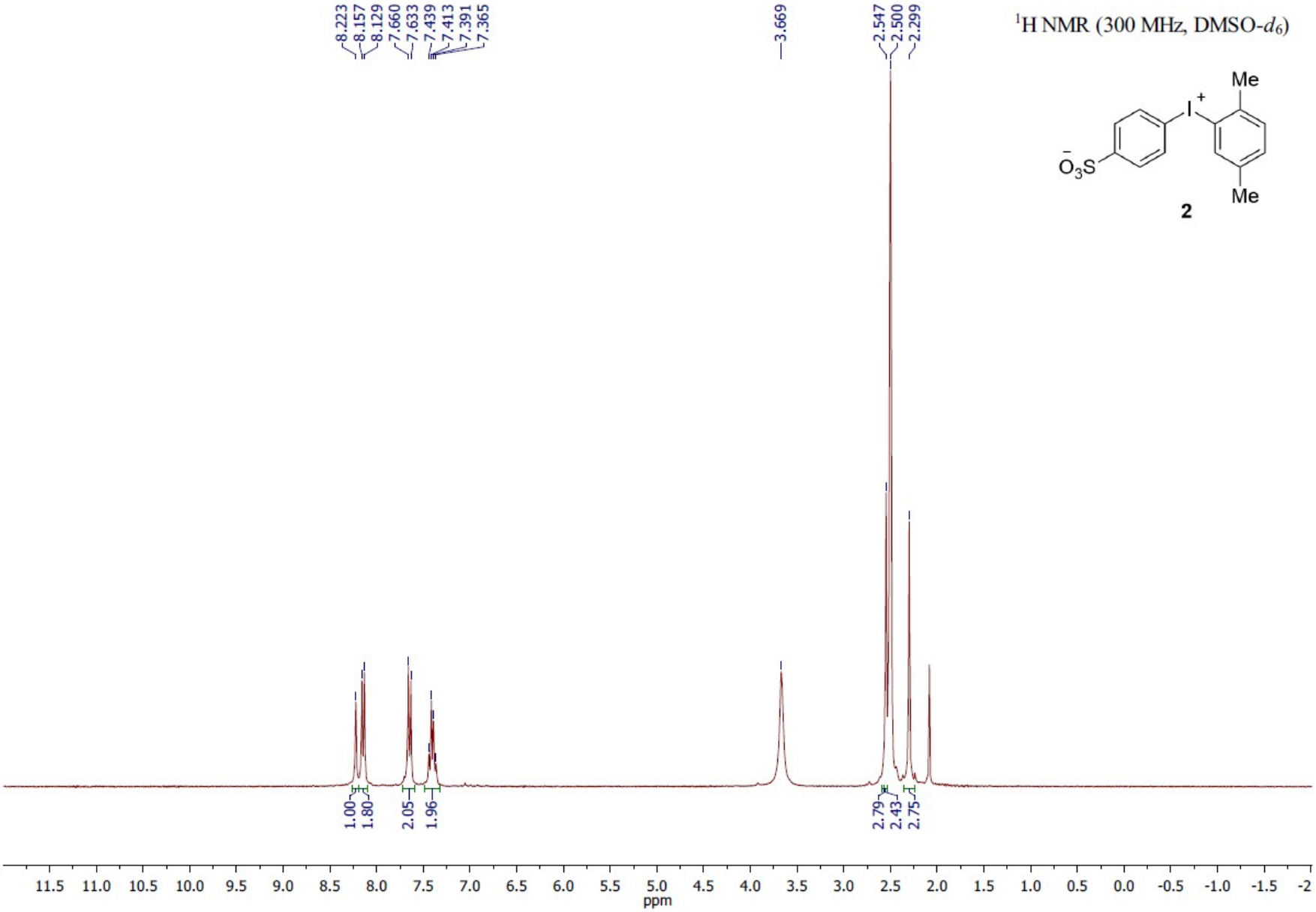

^{1}H NMR (300 MHz, DMSO-d_6)

2

^{13}C NMR (75 MHz, DMSO-d_6)

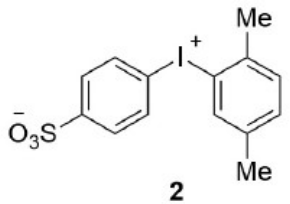

2

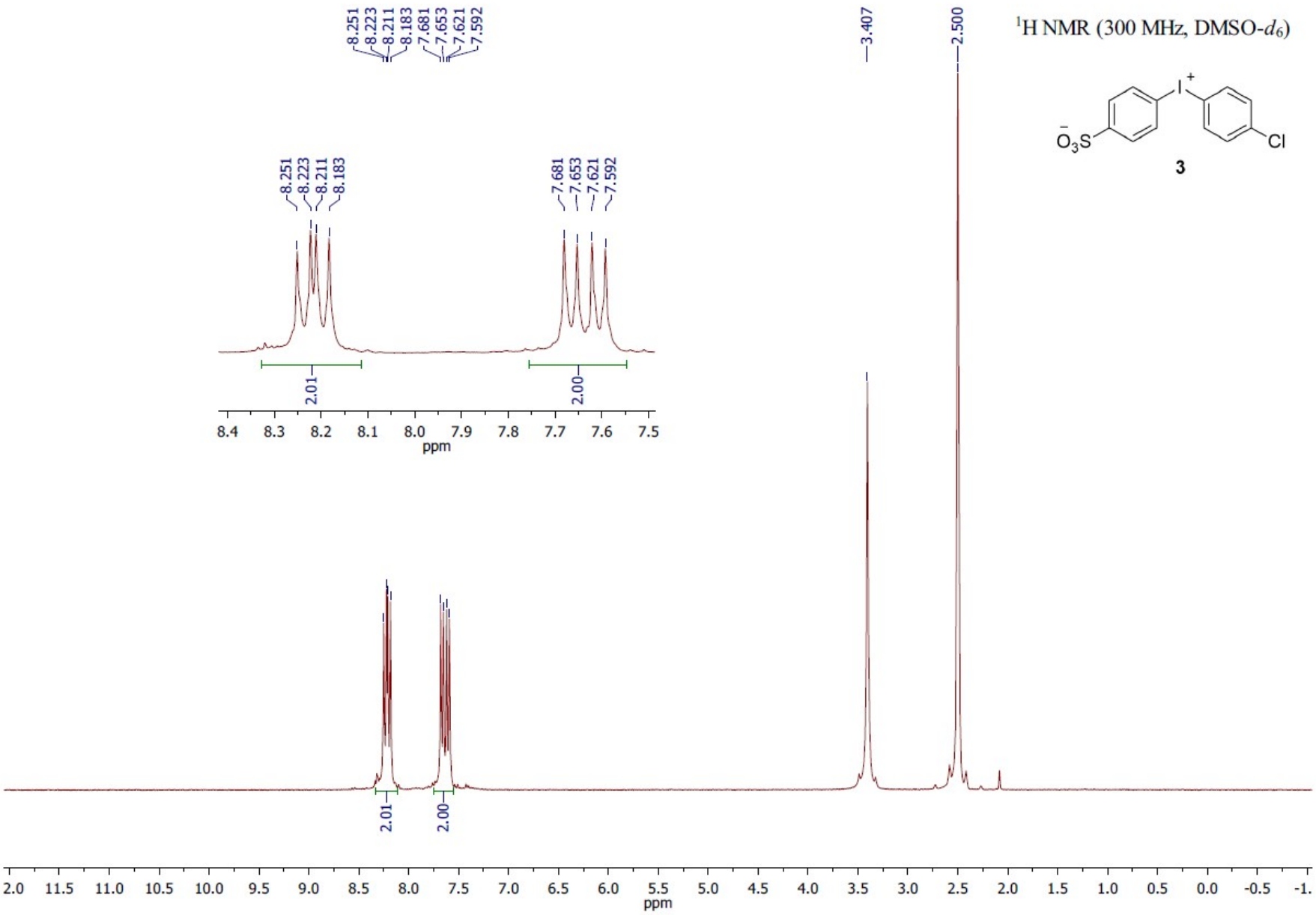
^{1}H NMR (300 MHz, DMSO-d_6)
3
8.251
8.223
8.211
8.183
7.681
7.653
7.621
7.592
3.407
2.500
2.01
2.00
ppm

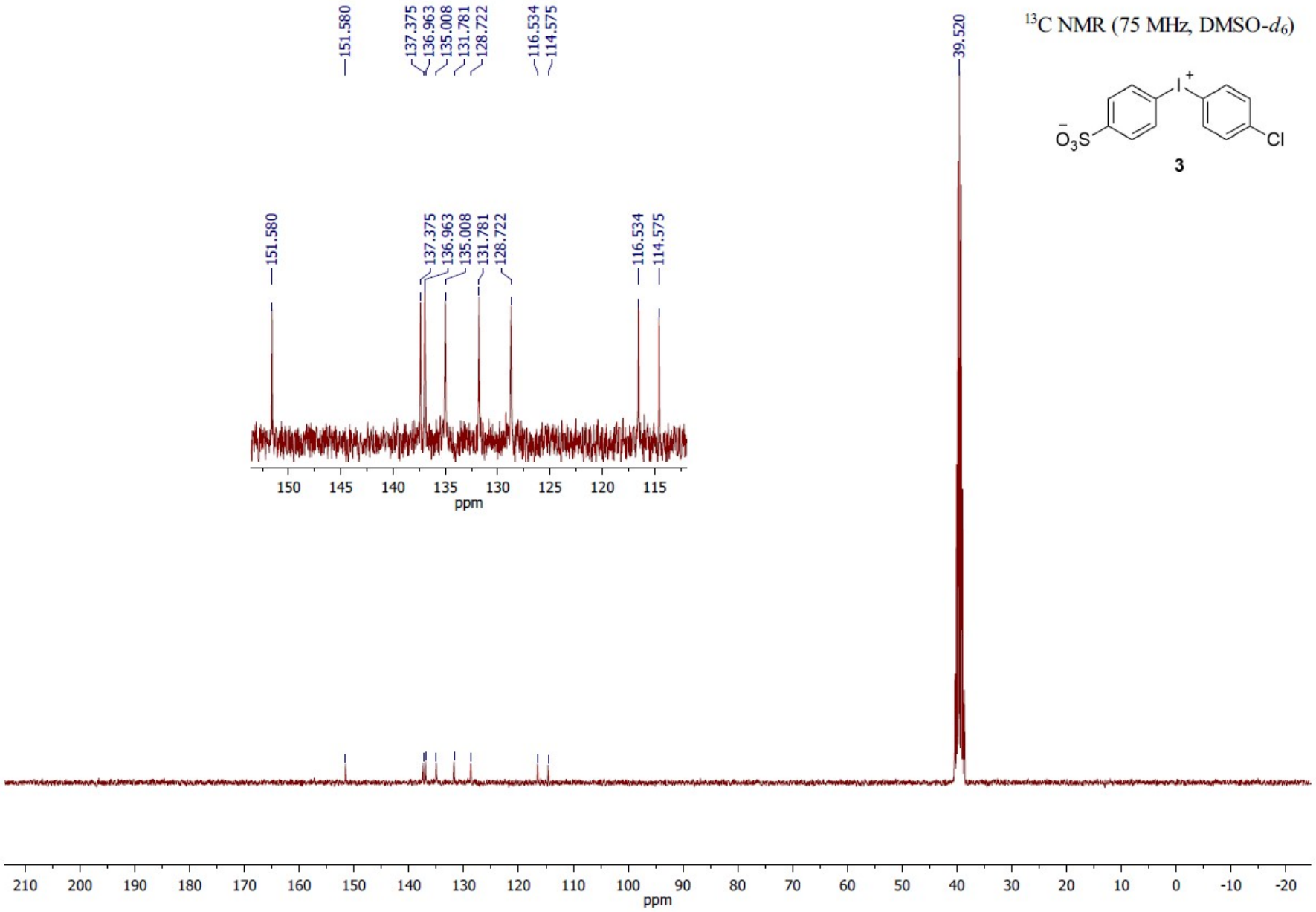
151.580
137.375
136.963
135.008
131.781
128.722
116.534
114.575
39.520
^{13}C NMR (75 MHz, DMSO-d_6)
O_3S
I
Cl
3
150 145 140 135 130 125 120 115
ppm
210 200 190 180 170 160 150 140 130 120 110 100 90 80 70 60 50 40 30 20 10 0 -10 -20
ppm